Journal of Sound and Vibration (2003) **259**(3), 637–648
doi:10.1006/jsvi.2002.5097, available online at http://www.idealibrary.com on IDEAL®

A NEW DYNAMIC MODELLING OF THE MAGNETIC TAPE RECORDING SYSTEM

J.-H. SUN AND R.-F. FUNG

Department of Mechanical and Automation Engineering, National Kaohsiung First University of Science and Technology, 1 University Road, Yenchau, Kaohsiung 824, Taiwan, Republic of China.
E-mail: rffung@ccms.nkfust.edu.tw

(*Received 2 July 2001, and in final form 8 April 2002*)

A new dynamic modelling of the tape vibration in a magnetic recording system is proposed by the concept that the length of the magnetic tape is divided into the entrance, head–tape coupling and exit regions. The main contribution of this paper is that the curvature effect of circular arc of the magnetic head is introduced in the dynamic formulation of the head–tape coupling region. The new separation spacing between the head and tape is defined. The steady state separation spacing and pressure distribution of foil film are compared for various curvatures of the magnetic head shape.
© 2002 Elsevier Science Ltd. All rights reserved.

1. INTRODUCTION

In order to further increase recording densities, new magnetic tapes are being used and continue to be developed for high-density magnetic recording applications [1–3]. The recording-density capability of the head element is highly dependent upon the head–tape interface [4]. The head–tape interface is a case of elastohydrodynamic lubrication in which we are faced with the solutions of two-coupled partial differential equations, the Reynolds equation and the elasticity equations describing the tape motion associated with the appropriate boundary conditions. A change in curvature with continuous slope has a marked effect on the film thickness. Theoretical prediction curves allow the calculation of the air gap as a function of the rate change of corner angle in the radius of curvature [5]. The tape displacements in the area above the head are coupled with the solution of the Reynolds equation. The film thickness (flying height) can be calculated between the head and tape. The simulated results for spherical heads were compared with the behavior of experimental systems by Greenberg [6]. Some peculiar characteristics affected by tape bending rigidity and tape wrap angle were found by Tanaka [7].

All the authors [5–7] were devoted to the solutions of the foil-bearing problem in which the flexible medium is wrapped around a circular cylinder. Recently, three-wavelength interferometry has been used successfully to measure the spacing for a digital linear tape interface [8] as well as a multi-module head–tape interface [9]. The correlation between head/tape spacing and asperity compliance of magnetic taper [10–12] has been investigated analytically and experimentally by using three-wavelength interferometry to measure the head/tape spacing and the contact spacing of metal particle tape as a function of contact pressure.

To the author's knowledge, no papers were focused on the curvature effect of circular arc of the magnetic head. The purpose of this paper is to propose a new dynamic modelling

0022-460X/02/$35.00 © 2002 Elsevier Science Ltd. All rights reserved.

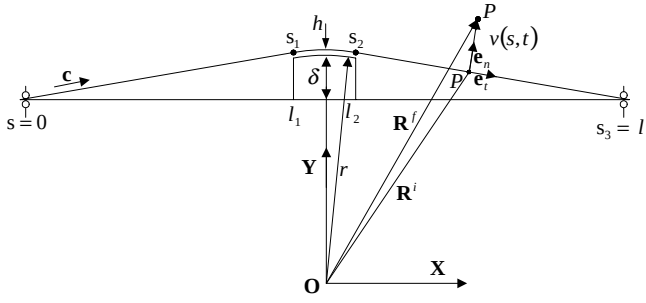

Figure 1. Physical configuration of the magnetic recording system.

describing the behavior between the fluid film and elastic deformation in the thin foil bearing. The Hamilton's principle and calculus of variation are employed to obtain the coupled equations and boundary conditions of the head–tape coupling problem. The string and beam models describing the magnetic tape are compared. The curvature effect of the magnetic head is considered in the dynamic formulation.

2. DERIVATION OF DYNAMIC EQUATIONS

Figure 1 shows the geometric configuration of the head–tape coupling system associated with the flexure rigidity EI, the initial tension T, and the constant velocity c. The tape travels across a cylindrical head with radius r. The tape length $s = s(t)$ is measured from the left-hand-side (LHS) support $s = 0$. The right-hand-side (RHS) support is placed at $s(t) = s_3$. The interval from $s = s_1$ to s_2 is the length of the head–tape coupling region. The interval from $s = 0$ to s_1 is called the entrance region while the interval from $s = s_2$ to s_3 is called the exit region.

2.1. GEOMETRY DESCRIPTION

In order to describe the geometry and the displacement relationship of the head–tape coupling system, a fixed co-ordinate system OXY is located at the circular center of the magnetic head and is shown in Figure 1. For the elastic tape, the position vector of any point P before deformation is

$$\mathbf{R}^i(s,t) = s\mathbf{e}_t, \quad 0 < s < s_3, \tag{1}$$

where $\mathbf{e}_t$ is the unit vector tangent to the tape at point P in the direction of increasing s. If the elastic tape is modelled by the beam theory, the displacement field is

$$\mathbf{U}(s,t) = -yv_s(s,t)\mathbf{e}_t + v(s,t)\mathbf{e}_n, \quad 0 < s < s_3, \tag{2}$$

where $\mathbf{e}_n$ is the unit vector in the normal direction, $v(s,t)$ is the transverse deflection of the tape at location s and it is positive in the positive $\mathbf{e}_n$ direction. Therefore, the position vector of point P after deformation is

$$\mathbf{R}^f(s,t) = \mathbf{R}^i(s,t) + \mathbf{U}(s,t). \tag{3}$$

Taking the total derivative of $\mathbf{R}^f(s,t)$ with respect to time, we obtain the absolute velocity as

$$\frac{\mathrm{d}\mathbf{R}^f(s,t)}{\mathrm{d}t} = \frac{\mathrm{d}\mathbf{R}^i(s,t)}{\mathrm{d}t} + \frac{\mathrm{d}\mathbf{U}(s,t)}{\mathrm{d}t}$$

$$= (c - ckv - ycv_{ss} - yv_{st})\mathbf{e}_t + (cv_s + v_t - yckv_s)\mathbf{e}_n, \tag{4}$$

where the travelling speed $\mathrm{d}s/\mathrm{d}t = c$ is used, $k = 1/r$ is the curvature of the head shape and can be obtained from $\mathrm{d}\mathbf{e}_t/\mathrm{d}s$, and r is the radius of the magnetic head. The terms including k are valid only for the head–tape coupling region throughout the paper. The kinetic energy (KE) of the tape becomes

$$KE = \frac{1}{2}\int_0^{s_3}\int_A \rho\left(\frac{\mathrm{d}\mathbf{R}^f}{\mathrm{d}t}\cdot\frac{\mathrm{d}\mathbf{R}^f}{\mathrm{d}t}\right)\mathrm{d}A\,\mathrm{d}s$$

$$= \begin{cases} \int \frac{1}{2}\rho[I(c^2v_{ss}^2 + v_{st}^2 + 2cv_{st}v_{ss} + c^2k^2v_s^2) + Ac^2(1 + k^2v^2 - 2kv + v_s^2) \\ \qquad + A(v_t^2 + 2cv_sv_t)]\,\mathrm{d}s, \quad s_1^+ > s > s_2^- \\ \int \frac{1}{2}\rho[I(c^2v_{ss}^2 + v_{st}^2 + 2cv_{st}v_{ss}) + Ac^2(1 + v_s^2) + A(v_t^2 + 2cv_sv_t)]\,\mathrm{d}s, \\ \qquad 0 < s < s_1^-,\ s_2^+ < s < s_3, \end{cases} \tag{5}$$

where ρ is the mass density, A is the cross-sectional area of the tape, and $I = \int_A y^2\,\mathrm{d}A$ and $\int_A y\,\mathrm{d}A = 0$ are used.

The engineering stain is

$$\varepsilon_E = \frac{|\mathrm{d}\mathbf{R}^f| - |\mathrm{d}\mathbf{R}^i|}{|\mathrm{d}\mathbf{R}^i|} = \left(\frac{\partial\mathbf{R}^f}{\partial s}\cdot\frac{\partial\mathbf{R}^f}{\partial s}\right)^{1/2} - 1$$

$$= -yv_{ss} - kv + \tfrac{1}{2}(1 - yk)^2v_s^2 + \text{H.O.T.}, \quad 0 < s < s_3. \tag{6}$$

The total strain energy is

$$S.E. = \int_V \left(\sigma_0\varepsilon_E + \frac{1}{2}E\varepsilon_E^2\right)\mathrm{d}V$$

$$= \begin{cases} \int \left[\frac{1}{2}E\left(Iv_{ss}^2 + Ak^2v^2 + Ik^2v_s^4 + \frac{1}{4}Av_s^4 + 2Ikv_s^2v_{ss} - Akvv_s^2\right)\right. \\ \left. + T\left(-kv + \frac{1}{2}v_s^2\right)\right]\mathrm{d}s, \quad s_1^+ < s < s_2^- \\ \int \frac{1}{2}\left(EIv_{ss}^2 + \frac{1}{4}EAv_s^4 + Tv_s^2\right)\mathrm{d}s, \quad 0 < s < s_1^-;\ s_2^+ < s < s_3, \end{cases} \tag{7}$$

where σ_0 is the initial stress, $T = \sigma_0 A$ and $\frac{1}{2}E\varepsilon_E^2$ are the terms due to the initial tension and the deflections which are measured from the initially tensioned configuration respectively. In equation (7), we neglect the high order terms $y^4v_{ss}^4, k^4v^4, 4y^2v_{ss}^2, 4k^2v^4, 4y^2k^2v^2v_{ss}^2$, and $(1 - yk)^4v_s^4$ in the strain energy.

Considering the virtual work done by the force due to the pressure difference in the head–tape region, we have

$$\delta W = (p - p_a) a \, \delta v_2, \quad s_1^+ < s < s_2^-, \tag{8}$$

where p is the pressure between the tape and head, p_a is the ambient air pressure, and a is the area of the head–tape coupling region.

2.2. HAMILTON'S PRINCIPLE.

For convenience, the subscripts 1, 2, and 3 of displacement v are used to represent the entrance, head–tape coupling and exit regions respectively. The Lagrangian functions $L_i, i = 1, 2, 3$ are the kinetic energy (5) minus the potential energy (7) in the entrance, head–tape coupling and exit regions respectively. It is seen that L_1 and L_3 are different only in the subscripts 1 and 3 of the displacement v. The curvature k exits only in the interval $s_1^+ < s < s_2^-$.

Considering the entire length $0 < s < s_3$ of the head–tape coupling system, Hamilton's principle can be written as

$$\int_{t_1}^{t_2} \left[\int_0^{s_1^-} \delta L_1 \, \mathrm{d}s + \int_{s_1^+}^{s_2^-} (\delta L_2 + \delta W) \, \mathrm{d}s + \int_{s_2^+}^{s_3} \delta L_3 \, \mathrm{d}s \right] \mathrm{d}t = 0, \tag{9}$$

where t_1 and t_2 are two arbitrary ending times. Only in the interval $s_1^+ < s < s_2^-$, the tape is subjected to the pressure force.

In the process of taking variation of equation (9), using the virtual relations of displacement and slope and collecting the like terms, we obtain the governing equations:

$$\rho A[v_{1,tt} + 2cv_{1,st} + c^2 v_{1,ss}] - Tv_{1,ss} - \tfrac{3}{2} EAv_{1,s}^2 v_{1,ss} + EIv_{1,ssss} = 0, \quad 0 < s < s_1^-, \tag{10a}$$

$$\rho A[v_{2,tt} - c^2 k^2 v_2 + c^2 k + 2cv_{2,st} + c^2 v_{2,ss}] - Tk + EAk^2 v_2 + \tfrac{1}{2} EAkv_{2,s}^2 - Tv_{2,ss}$$
$$- 6EIk^2 v_{2,s}^2 v_{2,ss} - \tfrac{3}{2} EAv_{2,s}^2 v_{2,ss} + EAkv_2 v_{2,ss} + EIv_{2,ssss} = (p - p_a)a, \; s_1^+ < s < s_2^-, \tag{10b}$$

$$\rho A[v_{3,tt} + 2cv_{3,st} + c^2 v_{3,ss}] - Tv_{3,ss} - \tfrac{3}{2} EAv_{3,s}^2 v_{3,ss} + EIv_{3,ssss} = 0, \; s_2^+ < s < s_3 \tag{10c}$$

and the boundary conditions

$$v_1(0,t) = v_{1,ss}(0,t) = 0, \tag{11a,b}$$

$$[EIv_{1,ss}]_{s=s_1^-} = [EIv_{2,ss} + EIkv_{2,s}^2]_{s=s_1^+} \tag{11c}$$

$$[EIv_{1,sss}]_{s=s_1^-} = [-2EIk^2 v_{2,s}^3 + EAkv_2 v_{2,s} + EIv_{2,sss}]_{s=s_1^+} \tag{11d}$$

$$[EIv_{2,ss} + EIkv_{2,s}^2]_{s=s_2^-} = [EIv_{3,ss}]_{s=s_2^+} \tag{11e}$$

$$[2EIk^2 v_{2,s}^3 - EAkv_2 v_{2,s} + EIv_{2,sss}]_{s=s_2^-} = [EIv_{3,sss}]_{s=s_2^+}, \tag{11f}$$

$$v_3(s_3,t) = v_{3,ss}(s_3,t) = 0. \tag{11 g, h}$$

$$v_1(s_1^-,t) = v_2(s_1^+,t), v_{1,s}(s_1^-,t) = v_{2,s}(s_1^+,t), \tag{11i, j}$$

$$v_2(s_2^-,t) = v_3(s_2^+,t), v_{2,s}(s_2^-,t) = v_{3,s}(s_2^+,t). \tag{11k, l}$$

The boundary conditions (11a, b) and (11g, h) are simply supported at $s = 0$ and s_3 respectively. The boundary conditions (11c, d) and (11e, f) describe the balances of the bending moment and shear force at $s = s_1$ and s_2 respectively. The continuous conditions [13] shown in equations (11i, j) and (11k, l) imply that the points just before and after the LHS and RHS points $s = s_1$ and s_2 have the same displacement and slope respectively. The 12 boundary conditions (11a–l) are enough to solve the three governing equations (10a–c). All the above motion equations and boundary conditions are based on the Euler–Bernoulli beam theory [14], and the rotary-inertia ρI term is not considered in equations (10) and (11).

2.3. TRAVELLING STRING MODEL

If all the terms containing EA and k are eliminated, the equation becomes

$$\rho A[v_{,tt} + 2cv_{,st} + c^2 v_{,ss}] - Tv_{,ss} + EIv_{,ssss} = (p - p_a)a\{\mathrm{H}(s - s_1) - \mathrm{H}(s - s_2)\}, \tag{12}$$

where H is the Heaviside function, and the boundary conditions are

$$v(s_1, t) = v_{ss}(s_1, t) = 0, \tag{13a, b}$$

$$v(s_3, t) = v_{ss}(s_3, t) = 0. \tag{13c, d}$$

Equations (12) and (13) are the same as those of beam model studied by Stahl *et al.* [15], Granzow and Lebeck [16], and Wickert [17].

The travelling string model can be reduced from the Euler–Bernoulli beam theory by eliminating the flexural rigidity EI and the non-linear terms in equations (10) and (11). Therefore, the linear governing equations become

$$\rho A[v_{1,tt} + 2cv_{1,st} + c^2 v_{1,ss}] - Tv_{1,ss} = 0, \tag{14a}$$

$$\rho A[v_{2,tt} - c^2 k^2 v_2 + c^2 k + 2cv_{2,st} + c^2 v_{2,ss}] - Tk - Tv_{2,ss} = (p - p_a)a, \tag{14b}$$

$$\rho A[v_{3,tt} + 2cv_{3,st} + c^2 v_{3,ss}] - Tv_{3,ss} = 0. \tag{14c}$$

Equations (14a–c) can be compounded into

$$\rho A[v_{,tt} + 2cv_{,st} + c^2 v_{,ss}] - Tv_{,ss} = [(p - p_a)a + \rho Ac^2 k^2 v - \rho Ac^2 k + Tk]\{H(s - s_1) - H(s - s_2)\}, \tag{15}$$

where $2\rho Acv_{,st}$ is due to the Coriolis acceleration, $\rho Av_{,tt}$ is due to the inertial acceleration, and $\rho c^2 Av_{,ss}$ is the acceleration term due to the travelling speed. The three terms, $\rho Ac^2 k^2 v$,$\rho Ac^2 k$ and Tk, are the transverse forces due to the effect of the curvature. If the curvature effect in equation (15) is eliminated, it is the same as that studied by Lakshmikumaran and Wickert [18].

The boundary conditions (11) can be simplified as

$$v(s_1, t) = v(s_3, t) = 0. \tag{16a, b}$$

2.4. REYNOLDS EQUATION

In all the previous studies [15–18], the displacement $v(x, t)$ defined in Figure 2(a) is measured from the x-axis and the separation spacing between the head and tape is

$$h(x, t) = v(x, t) - \delta(x), \quad x_1 < x < x_2. \tag{17}$$

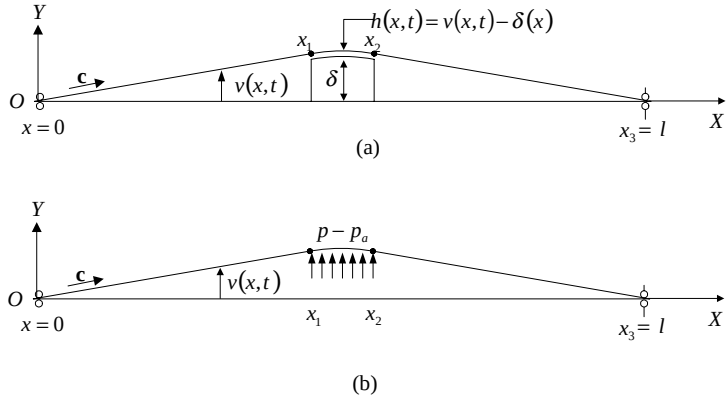

Figure 2. (a) The previous physical model of the magnetic recording system; (b) the previous magnetic recording system forced by the pressure ($p - p_a$).

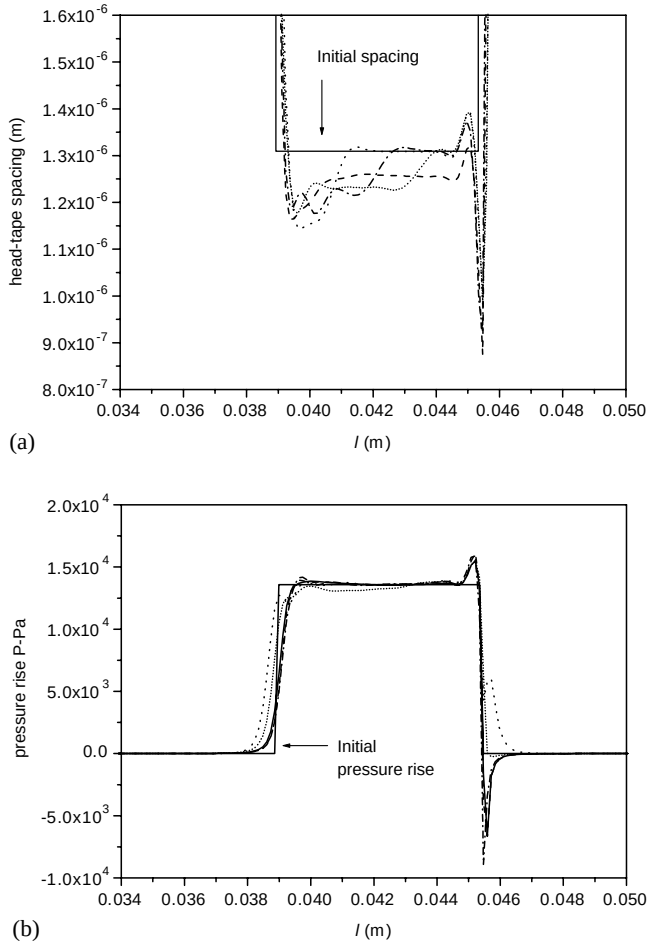

Figure 3. (a) Developments of steady state tape spacing; (b) developments of steady state pressure rise solutions: (…, 1 ms, —·—·, 2 ms, ···, 3 ms, – – –, 10 ms, and ——, 1 s).

TABLE 1

The parameters of the head–tape coupling system

Tape parameters	
EI/a(flexural rigidity)	$1{\cdot}52 \times 10^{-5}$ N m
$\rho A/a$(density)	$2{\cdot}07 \times 10^{-2}$ kg/m^2
T/a(tension)	$2{\cdot}77 \times 10^{2}$ N/m
c (velocity)	2·54 m/s
Lubrication parameters	
μ (viscosity)	$1{\cdot}81 \times 10^{-5}$ N s/m^2
p_a (ambient pressure)	$8{\cdot}41 \times 10^{4}$ N/m^2
λ_a (mean free path length at ambient pressure)	$6{\cdot}35 \times 10^{-8}$ m
Head and tape geometry	
l	$8{\cdot}34 \times 10^{-2}$ m
l_1	$3{\cdot}47 \times 10^{-2}$ m
l_2	$4{\cdot}97 \times 10^{-2}$ m
r(radius)	$2{\cdot}04 \times 10^{-2}$ m
$\delta(s)$ is a circular arc	
$\delta_{\max}$	$6{\cdot}35 \times 10^{-3}$ m
Finite difference parameters	
Δt	1×10^{-6} s
Δx	$1{\cdot}27 \times 10^{-4}$ m

In these studies, the magnetic tape is subjected to the pressure rise $(p - p_a)$ as shown in Figure 2(b), and the curvature effect of the head shape was not considered.

In the present work, the new separation spacing between the head and tape shown in Figure 1 is defined as

$$h(s, t) = v(s, t), \quad s_1 \leqslant s \leqslant s_2. \tag{18}$$

This separation spacing is then used in the one-dimensional transient Reynolds equation to compute the pressure $p(s, t)$ in the air-bearing head–tape coupling region $s_1 \leqslant s \leqslant s_2$. The Reynolds equation [15] is

$$(h^3 p p_s)_s + 6\lambda_a p_a (h^2 p_s)_s = 6\mu c (ph)_s + 12\mu (ph)_t, \tag{19}$$

where λ_a is the mean free path length at the ambient air pressure p_a, and μ is the air viscosity.

In the entrance and exit regions, the pressure is the same as that of the ambient. The pressures are assumed to be ambient at the edges of head:

$$p(s_1, t) = p(s_2, t) = p_a. \tag{20}$$

The initial conditions for the air-bearing region within the tangent points are taken as

$$h(s,0) = 0.643 r (6\mu c/T)^{2/3}, \tag{21}$$

$$h_t(s, 0) = 0, \tag{22}$$

$$p(s, 0) = p_a + T/r. \tag{23}$$

They are the steady state solutions [15] of a perfectly flex foil wraps around a circular head of radius r. Two coupled transient equations (15) and (19) subjected to their corresponding boundary and initial conditions must be solved simultaneously.

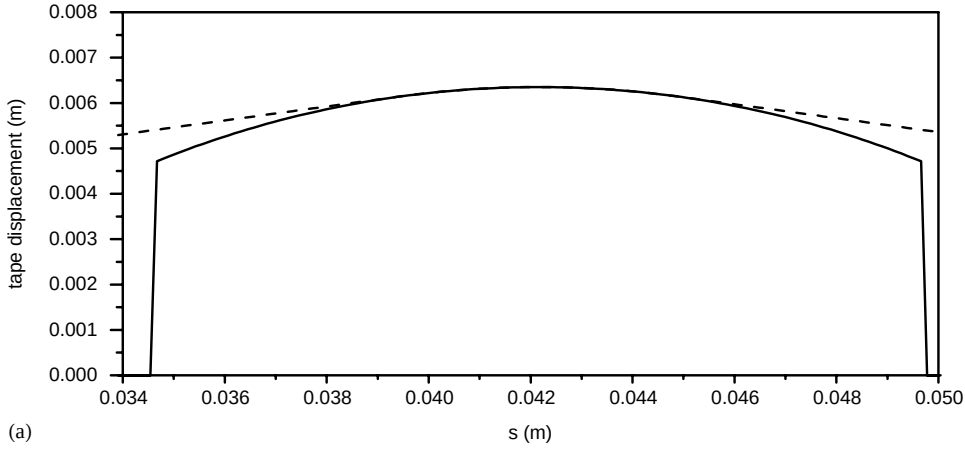

(a)

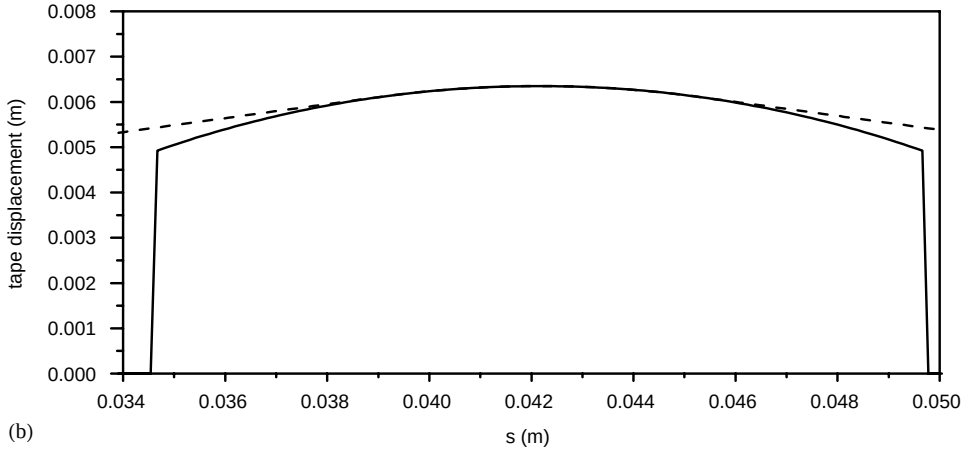

(b)

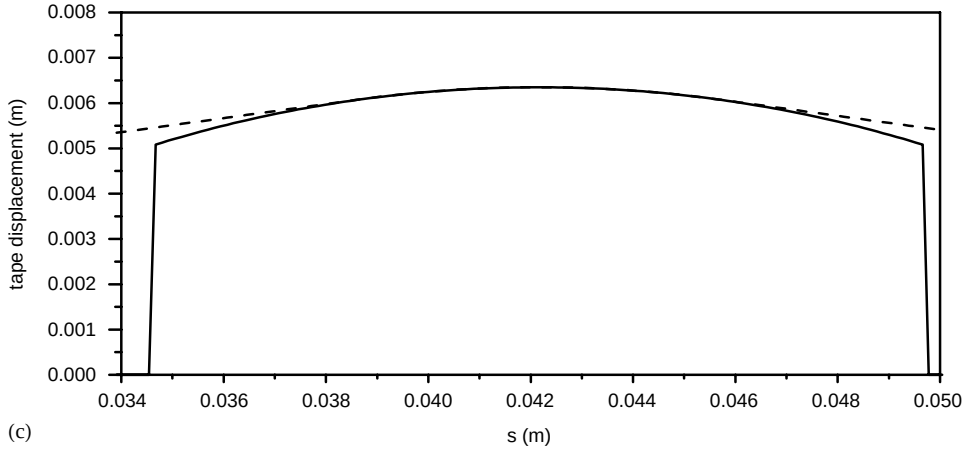

(c)

Figure 4. Geometric configurations of the magnetic recording systems. The tape initial shape (– – –) with the head geometric profile (——): (a) $r = 0{\cdot}018$ m; (b) $r = 0{\cdot}0192$ m; (c) $r = 0{\cdot}0204$ m.

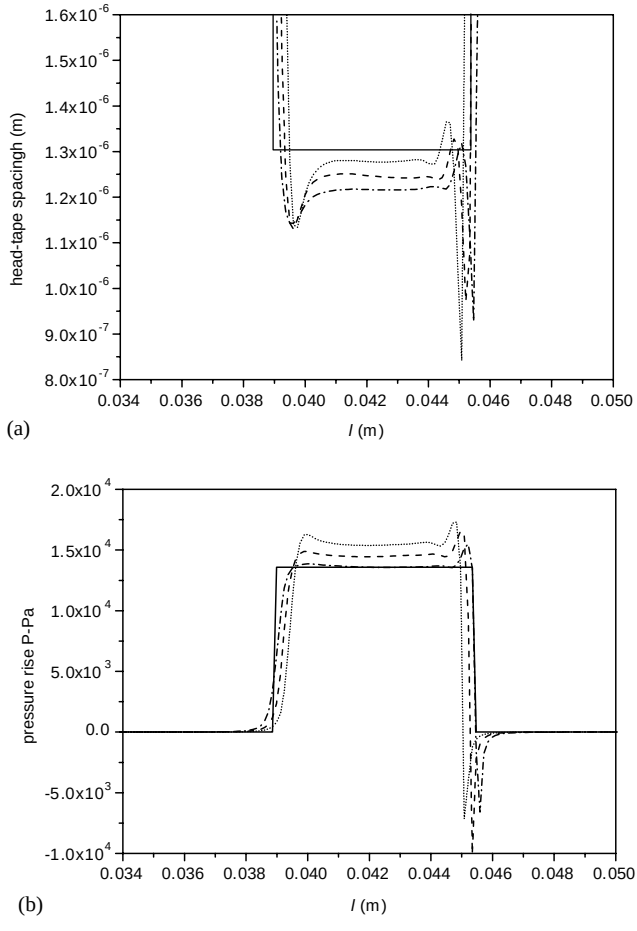

Figure 5. (a) The steady state head–tape spacing with different radii; (b) the steady state pressure rise with different radii; $\cdots$, $r = 0{\cdot}018$ m; – – –, $r = 0{\cdot}0192$ m; (–·–·–·), $r = 0{\cdot}0204$ m.

3. NUMERICAL RESULTS

The numerical results of tape vibration equation (15) for the string model and Reynolds equation (19) are solved simultaneously by finite difference method. To accomplish this, a uniform grid of mesh $\Delta(s)$ is imposed on the spatial domain $0 \leqslant s \leqslant s_3$, while the time domain is discretized by a time step $\Delta(t)$. Equation (19) is solved first for $h(s, t)$ at a given time step, and then the solution of the advanced time step of equation (15) is solved. This process is repeated for successive time steps.

The appropriate space and time steps, $\Delta(s)$ and $\Delta(t)$, must be determined first by numerical experiments. The most critical is the value of $\Delta(t)$. We find that the solutions of the equations are stable for value of $\Delta(t)$ substantially larger than that required for accuracy. To determine a suitable value of $\Delta(t)$ for a given choice of $\Delta(s)$, a steady state solution is calculated using a relatively large value of $\Delta(t)$. Next, the solution was continued for a smaller $\Delta(t)$. If the steady state is achieved in the first run substantially, the solution is continued for the smaller $\Delta(t)$. In all the cases, only one or two refinements of $\Delta(t)$ are necessary to find and cause no change in the steady state solution. Finally, the problem is

rerun from the initial state using the value $\Delta(t)$ as found above. In a case of the steady state solution obtained in the final run, the time step $\Delta(t)$ agrees with that obtained by the refinement [15].

The first attempt is to solve the coupled system for the solution converging to a steady state solution. Figures 3(a, b) illustrate the transient approach for a typical case, where the numerical results of the various final times 1, 2, 3, 10 ms, and 1·0 s are compared. Table 1 lists the parameters in the numerical experiments.

In this paper, we are interested to investigate the curvature effect of a wide self-acting foil-bearing geometry profile. The foil enters and exits through the tape guides and a bearing contour is positioned between the foil boundary conditions ($s_1 < s < s_2$). Figures 4 (a, b, c) show, respectively, the geometric configurations of different radii: $r = 0{\cdot}018$ m with $s_1 = 0{\cdot}03937$ m and $s_2 = 0{\cdot}044958$ m, $r = 0{\cdot}0192$ m with $s_1 = 0{\cdot}039116$ m and $s_2 = 0{\cdot}045212$ m and $r = 0{\cdot}0204$ m with $s_1 = 0{\cdot}038989$ m and $s_2 = 0{\cdot}045339$ m. Figures 5(a, b) compare the steady state head–tape spacing and pressure rise for the different curvatures ($k = 1/r$, $r = 0{\cdot}018$ m, $r = 0{\cdot}0192$ m, and $r = 0{\cdot}0204$ m) at the final time $t = 1$ s. It is seen that as the curvature of the head shape increases, the head–tape spacing and the pressure rise increase, and the head–tape coupling region decreases.

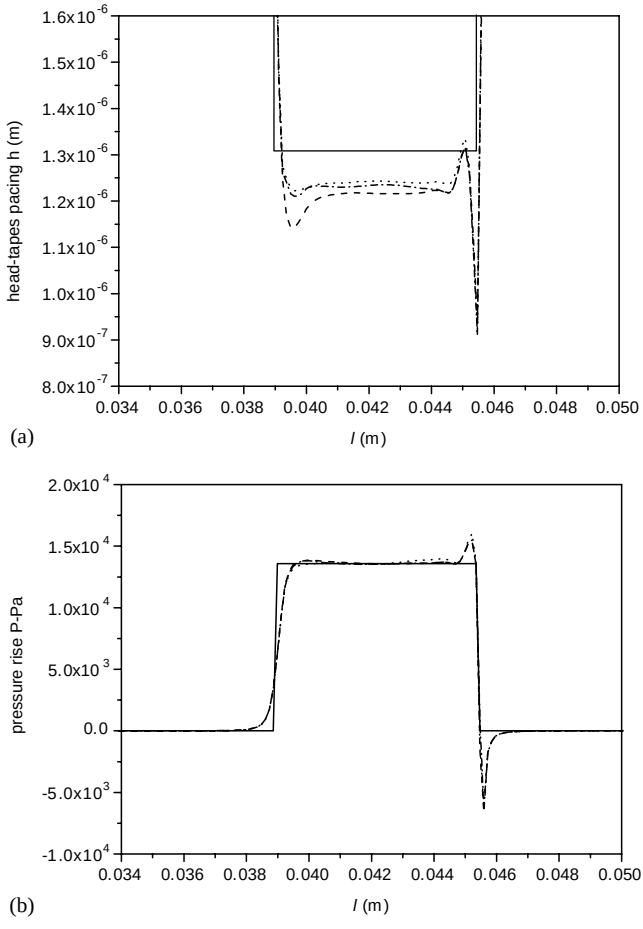

Figure 6. (a) The steady state head–tape spacing; (b) the steady state pressure rise with different flexural rigidities: ···, $EI/a = 7{\cdot}6 \times 10^{-5}$ N m; –·–·–, $EI/a = 1{\cdot}52 \times 10^{-5}$ N m; – – –, $EI/a = 0$ N m.

At last, we compared the steady-state solutions between the Euler–Bernoulli beam and string theories of the magnetic tape. For the beam model, the bending term $EIv_{,ssss}$ must be added at the LHS of equation (15). In Figures 6(a,b), the results of the head–tape spacing and pressure rise with different flexural rigidities ($EI/a = 1{\cdot}52 \times 10^{-5}$, $7{\cdot}6 \times 10^{-5}$ and 0 N m) are compared respectively. It is found that as the flexural rigidity increases, the head–tape spacing increases. However, the pressure rise does not increase significantly.

4. CONCLUSIONS

The Hamilton's principle and calculus of variation are successfully employed to derive the governing equations and the boundary conditions of the head–tape coupling system. In the new dynamic modelling, the magnetic tape is divided into the entrance, head–tape coupling and exit regions. In the head–tape coupling region, the curvature effect of circular arc of the magnetic head is included in the vibration analysis of the head–tape coupling system. Numerical results for the steady state head–tape spacing and pressure rises are compared for different curvatures of head shapes. It is found that as the curvature of the head shape increases, the head–tape coupling region decreases, and the head–tape spacing and pressure rise increase in the tape–head coupling region.

ACKNOWLEDGMENTS

The authors are greatly indebted to the National Science Council for the support of the research through Contract No. NSC 90-2213-E-033-019.

REFERENCES

1. B. BHUSHAN 1992 *Mechanics and Reliability of Flexible Magnetic Media*. New York: Springer-Verlag.
2. B. BHUSHAN 1996 *Tribology and Mechanics of Magnetic Storage Devices*. New York: Springer-Verlag, second edition.
3. C. D. MEE and E. D. DANIEL 1996 *Magnetic Recording Technology*. New York: McGraw-Hill, second edition.
4. S. T. PATTON and B. BHUSHAN 1998 *IEEE Transactions on Magnetics* **34**, 575–587. Effect of diamond-like carbon coating and surface topography on the performance of metal evaporated magnetic tapes.
5. A. ESHEL 1970 *Journal of Lubrication Technology, Transactions of the American Society of Mechanical Engineers* **91**, 359–362. On controlling the film thickness in self-acting foil bearing.
6. H. J. GREENBERG 1979 *IBM Journal of Research and Development* **23**, 197–205. Study of head-tape interaction in high speed rotating head recording.
7. K. TANAKA 1985 *Tribology and Mechanics of Magnetic Storage Systems, ASLE* SP-19, 72–79. Analytical and experiment study of tape spacing for magnetic tape unit—effects of tape bending rigidity, gas compressibility, and molecular mean free path.
8. S. TAN, B. GARRETTSON, F. E. TALKE, D. KNEEBURG and J. JUDGE 1999 *STLE Tribology Transactions* **19**, 201–210. Head/tape spacing measurement for digital linear tape drives using three-color interferometry.
9. B. GARRETTSON, S. TAN and F. E. TALKE 1999 T*he International Magnetism Conference, Kyongju, Korea*. Effect of slot edge defects on the head/tape spacing.
10. S. W. TAN, E. BAUGH and F. E. TALKE 1999 *Journal of Tribology, Transactions of the American Society of Mechanical Engineers* **121**, 121–127. Improve method for the measurement of asperity compliance of magnetic tapes.
11. S. W. TAN and F. E. TALKE 1999 *IEEE Transactions on Magnetics* **35**, 770–775. Experimental investigations of asperity compliance of flexible magnetic medium.

12. S. W. TAN and F. E. TALKE 1999 *IEEE Transactions on Magnetics* **35**, 2382–2384. Correlation between head/tape spacing and asperity compliance of magnetic tapes.
13. J. M. GEAR and S. P. TIMOSHENKO 1984 *Mechanics of Materials*, 736. Belmont, CA: Wadsworth Inc., second edition.
14. S. CHOURA and S. JAYAASURIYA, 1991 *Journal of Dynamic Systems, Measurement & Control, Transactions of the American Society of Mechanical Engineers* **113**, 26–33. On the modeling, and open-loop control of a rotating thin flexible beam.
15. K. J. STAHL, J. W. WHITE and K. L. DECKERT 1974 *IBM Journal of Research and Development* **18**, 513–520. Dynamic response of self-acting foil bearings.
16. G. D. GRANZOW and A. O. LEBECK, 1984 *Tribology and Mechanics of Magnetic Storage Systems, ASLE* SP-16 54–58. An improved one-dimensional foil bearing solution.
17. J. A. WICKERT 1993 *Journal of Vibration and Acoustics, Transactions of the ASME* **115**, 145–151. Free linear vibration of self-pressurized foil bearings.
18. A. V. LAKSHMIKUMARAN and J. A. WICKERT, 1996 *Journal of Vibration and Acoustics, Transactions of the American Society of Mechanical Engineers* **118**, 398–405. On the vibration of coupled traveling string and air bearing systems.